Published OnlineFirst August 30, 2011; DOI:10.1158/1078-0432.CCR-11-1054

Clinical Cancer Research

The Novel Chemical Entity YTR107 Inhibits Recruitment of Nucleophosmin to Sites of DNA Damage, Suppressing Repair of DNA Double-Strand Breaks and Enhancing Radiosensitization

Konjeti R. Sekhar, Yerramreddy Thirupathi Reddy, Penthala Narsimha Reddy, et al.

Clin Cancer Res 2011;17:6490-6499. Published OnlineFirst August 30, 2011.

Published OnlineFirst August 30, 2011; DOI:10.1158/1078-0432.CCR-11-1054

Cancer Therapy: Preclinical

Clinical Cancer Research

The Novel Chemical Entity YTR107 Inhibits Recruitment of Nucleophosmin to Sites of DNA Damage, Suppressing Repair of DNA Double-Strand Breaks and Enhancing Radiosensitization

Konjeti R. Sekhar[1], Yerramreddy Thirupathi Reddy[4], Penthala Narsimha Reddy[4], Peter A. Crooks[4,6], Amudhan Venkateswaran[1], William Hayes McDonald[2], Ling Geng[1], Soumya Sasi[1], Robert P. Van Der Waal[5], Joseph L. Roti Roti[5], Kenneth J. Salleng[3], Girish Rachakonda[1], and Michael L. Freeman[1]

Abstract

Purpose: Radiation therapy continues to be an important therapeutic strategy for providing definitive local/regional control of human cancer. However, oncogenes that harbor driver mutations and/or amplifications can compromise therapeutic efficacy. Thus, there is a need for novel approaches that enhance the DNA damage produced by ionizing radiation.

Experimental Design: A forward chemical genetic approach coupled with cell-based phenotypic screening of several tumor cell lines was used to identify a novel chemical entity (NCE) that functioned as a radiation sensitizer. Proteomics, comet assays, confocal microscopy, and immunoblotting were used to identify the biological target.

Results: The screening process identified a 5-((*N*-benzyl-1*H*-indol-3-yl)-methylene)pyrimidine-2,4,6 (1*H*,3*H*,5*H*)trione as an NCE that radiosensitized cancer cells expressing amplified and/or mutated *RAS*, *ErbB*, *PIK3CA*, and/or *BRAF* oncogenes. Affinity-based solid-phase resin capture followed by liquid chromatography/tandem mass spectrometry identified the chaperone nucleophosmin (NPM) as the NCE target. SiRNA suppression of NPM abrogated radiosensitization by the NCE. Confocal microscopy showed that the NCE inhibited NPM shuttling to radiation-induced DNA damage repair foci, and the analysis of comet assays indicated a diminished rate of DNA double-strand break repair.

Conclusion: These data support the hypothesis that inhibition of DNA repair due to inhibition of NPM shuttling increases the efficacy of DNA-damaging therapeutic strategies. *Clin Cancer Res; 17(20); 6490–9. ©2011 AACR.*

Introduction

Cytotoxic therapy continues to be a very important tool for the treatment of human cancer. Ionizing radiation is an example of a cytotoxic agent that has a central role in cancer therapy and is used to provide local/regional control of prostate, pancreatic, head and neck, breast, brain, colorectal, lung, metastatic bone, Hodgkin, ovarian, and uterine cancers (2).

DNA damage stress overload is a concept that describes the ability of a therapeutic regime to overwhelm the DNA damage response pathways in a cancer cell (1). This concept helps explain the efficacy of ionizing radiation, which produces DNA double-strand breaks (DSB), single-strand breaks, and base modifications (3) due to generation of oxygen radicals. The predominant radical yield following X-ray or γ-irradiation consists of hydroxyl and superoxide anion radicals (discussed in ref. 4) and it is the hydroxyl radical that leads to the formation of toxic DNA DSBs.

Emerging research has shown that cancer driver mutations can impact a cell's response to radiation-induced DNA damage (5, 6). Driver mutations are defined as mutations that initiate and sustain tumor progression (1). Tumors may express several driver mutations (7) and each can independently affect compensatory DNA damage response pathways. Colorectal cancer provides an excellent example. A colorectal

Authors' Affiliations: Departments of [1]Radiation Oncology and [2]Biochemistry, [3]Division of Animal Care, Vanderbilt University School of Medicine, Nashville, Tennessee; [4]Department of Pharmaceutical Sciences, College of Pharmacy, University of Kentucky, Lexington, Kentucky; and [5]Department of Radiation Oncology, Washington University School of Medicine, St. Louis, Missouri, [6]Department of Pharmaceutical Sciences, University of Arkansas for Medical Sciences. Little Rock, Arkansas.

Note: Supplementary data for this article are available at Clinical Cancer Research Online (http://clincancerres.aacrjournals.org/).

Corresponding Author: Michael L. Freeman, B902 TVC, Department of Radiation Oncology, Vanderbilt University School of Medicine/Vanderbilt-Ingram Cancer Center, Nashville, TN 37232. Phone: 615-322-3606; Fax: 615-343-3061; E-mail: michael.freeman@vanderbilt.edu

doi: 10.1158/1078-0432.CCR-11-1054

Published OnlineFirst August 30, 2011; DOI:10.1158/1078-0432.CCR-11-1054

Translational Relevance

Ionizing radiation is an important tool for the treatment of human cancer, and it has been hypothesized that its effectiveness is a consequence of its ability to overload a cancer cell ability to respond to DNA damage (1). Emerging research has implicated the contribution of oncogenic driver mutations to radiation resistance. We hypothesized that the DNA damage stress overload paradigm could be exploited in cancer cells for the purpose of radiosensitization. A forward chemical genetics screen identified a novel chemical entity (NCE) that potentiated radiation sensitivity, as assayed in preclinical models. Radiosensitization was a consequence of increased DNA double-strand break (DSB) formation and repair inhibition. The NCE was used as a tool for target identification. This approach identified the chaperone NPM, a protein known to be required for DNA DSB repair. Confocal microscopy showed that the NCE prevented NPM shuttling to sites of DNA DSBs. These data identify the NPM shutting pathway as a potential target for enhancing the efficacy of DNA-damaging therapeutic strategies.

tumor may harbor a gain-of-function *KRAS* mutation and overexpress EGFR (8). Each of these mutations can independently confer a radiation resistance phenotype (9, 10) and negate therapeutic DNA damage stress overload strategies (1, 11). Thus, there is a need for novel approaches that enhance the DNA damage produced by cytotoxic agents.

We used a forward chemical genetic approach integrated with cell-based functional screening (12) to test the hypothesis that components of the DNA damage response pathway can be exploited for the purpose of radiosensitizing tumor cells expressing amplified and/or mutated oncogenes. A novel chemical library was synthesized and cell-based phenotypic assays were used (13) to screen for sensitivity to ionizing radiation. The screening process identified a 5-((*N*-benzyl-1*H*-indol-3-yl)methylene)pyrimidine-2,4,6(1*H*,3*H*,5*H*)trione, denoted as YTR107, as a compound that increased the number of DNA DSBs formed per Gy and slowed the repair of DNA DSBs.

Affinity-based solid-phase resin capture was then used for identifying potential biological targets. YTR107 linked to a solid-phase resin was used to capture cell lysate. Liquid chromatography/tandem mass spectrometry (LC/MS-MS) analysis of the captured protein identified the chaperone nucleophosmin (NPM) in the complex of proteins that bound to the affinity resin. Recombinant NPM was used to show that YTR107 can directly bind to NPM. NPM is a molecular chaperone involved in anaplastic large cell lymphoma (14), as well as in cellular processes such as centrosome duplication, ribosome biogenesis, cell-cycle progression (15), and repair of DNA damage (16). Phosphorylated T199 (pT199) NPM (pT199-NPM) shuttles to sites of DNA DSBs in an RNF8 dependent manner (16). Failure of pT199-NPM to localize to sites of DNA DSBs results in inhibition of their repair (16). We found that YTR107 inhibited NPM shuttling to ionizing radiation–induced DNA damage repair foci, as marked by γH2AX. Taken together, these results support the hypothesis that YTR107 inhibits DNA repair by inhibiting NPM shuttling and thus increases the efficacy of DNA-damaging therapeutic strategies.

Materials and Methods

Cell lines and reagents

Microplasma-free human HeLa cervical adenocarcinoma cells, HT29 colorectal adenocarcinoma cells, Panc-1 exocrine pancreatic cancer cells, MDA-MB-231 mammary adenocarcioma cells, HCC1806 breast adenocarcinoma cells, H460 non–small cell lung cancer (NSCLC) cells, and human D54 glioblastoma cells were grown in their recommended media. HT29 cells were grown as xenografts (as described in ref. 17). NSC348884 was obtained from the National Cancer Institute, NIH.

The following antibodies were used: RPA2 (Abcam), Chk1 (Santa Cruz Biotechnology), pS317 Chk1 (Cell Signaling Technology), pT199-NPM (Abcam), NPM (Invitrogen), and pS139 H2AX (Millipore). Carboplatin was purchased from Sigma-Aldrich.

Colony formation assay

Plating efficiency and colony formation were quantified as described in the work of Franken and colleagues (18).

Irradiation

Cells were inoculated into 100-mm Petri dishes and irradiated with a Mark 1 ^{137}Cs irradiator (2.0 Gy/min). A Pantek 300 kVp/10 mA X-ray machine (2.1 Gy/min) was used to irradiate xenograft tumors.

Synthetic chemistry

A series of (*Z*)-5-((*N*-benzyl-1*H*-indol-3-yl)methylene) imidazolidine-2,4-dione and 5-((*N*-benzyl-1*H*-indol-3-yl)methylene)pyrimidine-2,4,6(1*H*,3*H*,5*H*)trione derivatives that incorporate a variety of substituents in both the indole and *N*-benzyl moieties were synthesized (as described in ref. 13). Twenty-two compounds were synthesized and structurally characterized by ^{1}H and ^{13}C nuclear magnetic resonance spectroscopy, gas chromatography–mass spectroscopy, and elemental combustion analysis (13).

Comet assay

The neutral comet assay was carried out with the Comet Assay Kit from Trevigen following the manufacturer's instructions. CometScore software was used to analyze the comets.

PARP activity

PARP activity was measured with a kit from Trevigen following the manufacturer's instructions.

Published OnlineFirst August 30, 2011; DOI:10.1158/1078-0432.CCR-11-1054

Immunofluorescence

Lab-Tek II chamber slides (Nalge Nunc International) were used as a platform for cell growth. HeLa cells were grown to 50% confluency and treated with YTR107 (50 μmol/L) for 30 minutes before exposure to 4 Gy radiation. Cells were then allowed to grow for 1.5 hours at 37°C before fixing with cold 4% paraformaldehyde at 4°C for 20 minutes. Dimethyl sulfoxide (DMSO) was used as the solvent control. Paraformaldehyde-fixed cells were permeabilized by treatment with 0.1% Triton X-100 in PBS. Cells were then blocked in 3% bovine serum albumin in PBS for 1 hour at 25°C. pNPM rabbit monoclonal (Abcam) and γH2AX mouse polyclonal antibodies (Millipore) were then applied at 1:200 dilutions in 1× BSA overnight at 4°C and subsequently labeled with Alexa 647 or Alexa 486 fluorescent dye–conjugated secondary antibodies, respectively. 4′,6-Diamidino-2-phenylindole (DAPI; Invitrogen) was used as the nuclear stain. Images were acquired on an Olympus FV 1000 inverted laser scanning confocal microscope.

Quantification of colocalized protein

Colocalization of pT199-NPM and γH2AX was quantified by the "Colocalization" module of Metamorph software. Colocalization data were obtained from 84 cells per condition and represent 2 independent experiments.

Tumor growth inhibition

These studies were approved by the Vanderbilt Institutional Animal Care and Use Committee and done under guidelines outlined in The Guide for the Care and Use of Laboratory Animals. Hindlimbs of homozygous *nu/nu* athymic nude mice (Charles River Laboratories), approximately 6 to 8 weeks of age, were subcutaneously implanted in HT29 human colorectal cancer cells. When tumors achieved a size of approximately 180 mm^3 [calculated 3 times per week according to the formula: length × $(width)^2$/2], they were randomized to the following protocols: 7 daily intraperitoneal injections of (a) DMSO (25 μL) or (b) 10 mg/kg of YTR107 in DMSO (25 μL) followed 30 minutes later by (c) 0 Gy or (d) 3 Gy exposure of X-rays (300 kVp/10 mA). Six mice were assigned to each protocol. Mice were shielded such that only the tumors were irradiated. Digital calipers were used to obtain the length and width of each tumor. The starting volume of each mouse was normalized to 1.0.

Proteomics

YTR107 and benzoic acid (control) were covalently linked to Dynabeads M-270 Amine (Invitrogen) in separate reactions. The structure of YTR107 containing a linker moiety is shown in Supplementary Fig. S4 and denoted as YTR119. Total protein lysate was prepared from HT29 cells in extraction buffer [1 mmol/L $CaCl_2$, 150 mmol/L NaCl, 10 mmol/L Tris, pH 7.4, 1% Triton X-100, and protease inhibitor cocktail (Sigma)]. An equal amount of protein lysate was added to the magnetic beads and incubated for 3 hours at 4°C with mixing. Unbound proteins were removed by magnetic separation; the beads were washed with TBS-T (20 mmol/L Tris, 150 mmol/L NaCl, 0.1% Triton X-100) 4 times. Bound proteins were eluted with elution buffer (20 mmol/L Tris, pH 8.0, 2mol/L NaCl). Proteins were resolved by SDS-PAGE and stained with colloidal Coomassie blue stain (Invitrogen). YTR107-specific proteins visualized by colloidal Coomassie blue staining were excised for identification by mass spectrometry. These bands were subjected to in-gel tryptic digestion, and the resulting peptides were analyzed by high-performance liquid chromatography coupled tandem mass spectrometry (LC/MS-MS). Briefly, peptides were resolved with an Eksigent 1D+ HPLC pump equipped with an AS1 autosampler on an 18-cm Jupiter (3 μm, 300 Å) 100-μm internal diameter, self-packed analytic column coupled directly to an LTQ (ThermoFisher) via a nanoelectrospray source. A full-scan mass spectrum followed by 5 data-dependent tandem mass spectra were collected throughout the run by dynamic exclusion to minimize acquisition of redundant spectra. MS/MS spectra were searched against a human protein database (UniprotKB v155) using SEQUEST (http://www.ncbi.nlm.nih.gov/pubmed/7741214), and results were filtered and collated using IDPicker (http://www.ncbi.nlm.nih.gov/pubmed/19522537).

Presence of NPM, the pulled down protein complex

Biotinylated YTR107 and biotinylated benzoic acid (PNR-4-31; structures shown in Supplementary Fig. S4) were synthesized and allowed to bind streptavidin magnetic beads (Promega) in 50% DMSO in PBS. Unbound compounds were removed by washing with 50% DMSO and PBS. HT29 cell extract was prepared in radioimmunoprecipitation assay (RIPA) buffer (10 mmol/L Tris, pH 7.2, 150 mmol/L NaCl, 1% deoxycholic acid, 5 mmol/L EDTA, 1% Triton X-100, 0.1% SDS). Proteins were allowed to bind to the magnetic beads for 1 hour and washed 5 times with RIPA buffer and 3 times with RIPA buffer containing 500 mmol/L NaCl. The beads were heated with 15 μL of 5× Laemmli buffer and resolved on SDS-PAGE and Western blotted for NPM.

Recombinant NPM

Recombinant His-NPM was expressed from a pET28a vector, a generous gift from Dr. Jason Weber, Washington University) and purified with Ni-NTA agarose gel. Ten micrograms of NPM was added to biotinylated YTR107 or benzoic acid (control) bound to streptavidin magnetic beads as described earlier and incubated for 30 minutes while mixing at 4°C. The magnetic beads were washed 5 times to remove unbound protein, boiled with 5× Laemmli buffer, and immunoblotted for NPM.

Fractionating soluble and chromatin-bound nuclear protein

Preparation of nuclear extracts was done as described by Groisman and colleagues (19). In brief, cells in hypotonic buffer (10 mmol/L Tris-HCl, pH 7.3, 10 mmol/L KCl, 1.5 mmol/L $MgCl_2$, 10 mmol/L β-mercaptoethanol, and protease inhibitor cocktail) underwent Dounce homogenization.

Published OnlineFirst August 30, 2011; DOI:10.1158/1078-0432.CCR-11-1054

Nuclei were collected by centrifugation and resuspended in extraction buffer (15 mmol/L Tris-HCl, pH 7.3, 1 mmol/L EDTA, 0.4 mol/L NaCl, 1 mmol/L $MgCl_2$, 10% glycerol, 10 mmol/L β-mercaptoethanol, and protease inhibitor cocktail). After incubation for 30 minutes at 4°C, nuclei were centrifuged at 20,000 × *g* for 30 minutes (4°C). The supernatant was washed and subjected to immunoblotting.

Results

Cell-based phenotypic screening

The initial screening was done with human HT29 colorectal adenocarcinoma cells that express mutated *p53*, activated PIK3CA, and $BRAF^{V600E}$ (Supplementary Table S1). The cells also express amplified ErbB1 and wild-type HRAS. All screening was done using compound concentrations that did not reduce plating efficiencies below 70% following a 2-hour/37°C exposure. Radiosensitization was quantified from colony formation assays. Colony formation provides a rigorous test of cell viability, cell-cycle proliferation, and DNA damage sensitization by requiring individual cells to divide and proliferate through their cell cycle a minimum of 7 times after sustaining DNA damage (18).

Only 3 of the 22 compounds tested yielded statistically significant radiosensitization of cells exposed to 4 Gy (13). Compound YTR107 was 2-fold more effective than the other 2 radiosensitizing compounds ($P < 0.05$, Student *t* test) and therefore was chosen for further investigation (structure shown in Fig. 1). The dose–response curves and dose-modifying factors shown in Fig. 1 indicate that exposure to YTR107 significantly increased the radiation sensitivity of HT29 colorectal adenocarcinoma, D54 glioblastoma, PANC1 pancreatic carcinoma, MDA-MB-231 breast adenocarcinoma cells, and H460 NSCLC cells. Supplementary Table S1 lists known mutations present in these cancer cells. The dose-modifying factor shown in Fig. 1 is defined as the dose of radiation required to reduce survival to 10% in YTR107-treated cells divided by the dose of radiation required to reduce survival rate to 10% in cells treated with vehicle control.

An alternative method of comparing effectiveness is to compare survival produced by the clinically significant dose of 2 Gy. In HT29 cells, exposure to 2 Gy decreased survival to 0.79 ± 0.04 (SEM). Exposure to 25 μmol/L YTR107 plus 2 Gy reduced survival to 0.39 ± 0.04 (SEM; $P < 0.0001$, Student *t* test). Similar results were obtained in D54, PANC1, MDA-MB-231, and H460 cells when exposed to 25 μmol/L YTR107 plus 2 Gy ($P \leq 0.01$, Student *t* test).

YTR107 potentiates radiation-induced growth delay of HT29 tumor xenografts

HT29 tumor–bearing mice were administered 7 daily fractions of the following treatments: (i) intraperitoneal injection of solvent control DMSO; (ii) intraperitoneal

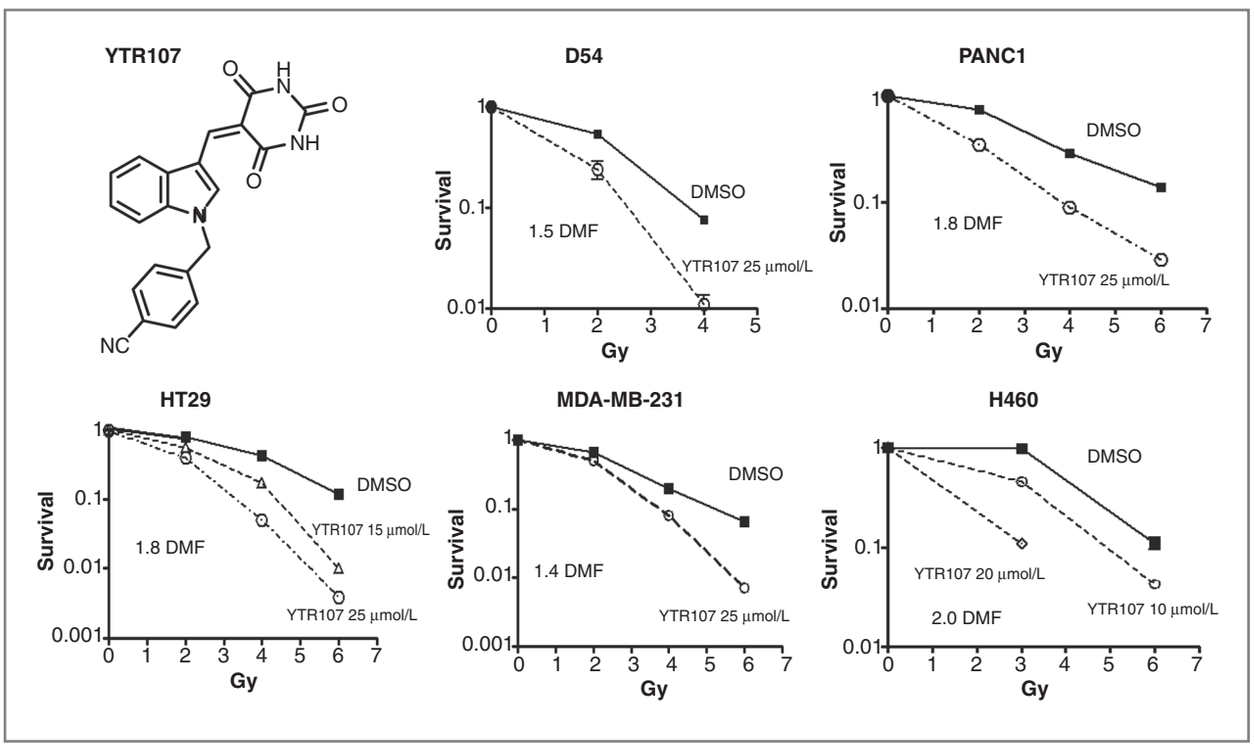

Figure 1. Radiation sensitivity is enhanced by exposure to YTR107. The chemical structure of YTR107 and the dose–response curves of D54, PANC1, HT29, MDA-MB-231, and H460 cells following X-ray irradiation. Cells were exposed to the indicated concentrations of YTR107 at 37°C for 30 minutes before, during, and 1.5 hours after irradiation. The dose-modifying factor (DMF) is defined as the dose of radiation required to reduce the survival rate to 10% in YTR107-treated cells divided by the dose of radiation required to reduce the survival rate to 10% in cells treated with vehicle control.

Published OnlineFirst August 30, 2011; DOI:10.1158/1078-0432.CCR-11-1054

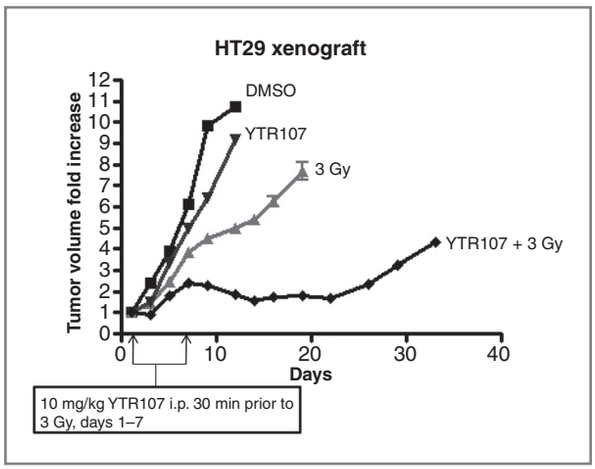

Figure 2. Tumor growth delay following treatment with YTR107 plus irradiation. Athymic *nu/nu* mice with HT29 hindlimb tumors received daily intraperitoneal (i.p.) injections of DMSO or 10 mg/kg of YTR107 for 7 consecutive days, followed 30 minutes later by the administration of 0 or 3 Gy.

injection of 10 mg/kg of YTR107 (every 7 days); (iii) intraperitoneal injection of solvent control followed 30 minutes later with 3 Gy (every 7 days); (iv) intraperitoneal injection of 10 mg/kg of YTR107 followed 30 minutes later by 3 Gy (every 7 days). The fold increase in tumor volume is shown in Fig. 2. In untreated mice, tumor volume increased 4-fold in 5 days. In mice administered YTR alone, tumor volume increased 4-fold in 6 days. In mice administered 7 daily 3 Gy fractions, tumor volume increased 4-fold in 7 days. However, in mice administered 7 daily fractions consisting of YTR107 followed by 3 Gy, it took 32 days for tumor volume to increase 4-fold. An alternative method of comparison was also used. Twelve days after irradiation (19th day of experiment; Fig. 2), tumor volume increased 7.7-fold ± 1.0 (SEM) for irradiation alone versus 1.8-fold ± 0.24 (SEM) for tumors administered YTR107 plus irradiation ($P = 0.001$, Student t test).

It is important to reiterate that radiosensitization by this NCE occurred at concentrations that did not lower the plating efficiency of the cell-based assays below 70% compared with solvent control. Furthermore, YTR107 was well tolerated in mice. Five female C57BL/6J mice were intraperitoneally administered 10 mg/kg YTR107 for 5 consecutive days, and 5 mice were administered solvent alone. Thirty-five days after injection, mice were euthanized and subjected to necropsy by a veterinarian trained in veterinary pathology. Gross and histologic examination of liver, lung, thymus, heart spleen, cerebellum, pancreas, small intestine, kidney, and adrenal gland did not reveal evidence of toxicity that could be attributed to injection of YTR107 (data not shown). Both a complete blood count and a white blood cell differential count were done. No significant differences were noted (Supplementary Table S2). The weights of the mice measured over the 35-day interval are shown in Supplementary Figure S1. There was not a statistically significant difference in weights of mice administered the 2 treatments ($P > 0.05$, Student t test). We interpret these data to indicate that the change in radiosensitization cannot be considered a secondary consequence of toxicity.

Replication stress

The data shown in Fig. 3A show that incorporation of [^{3}H]thymidine into trichloroacetic acid–precipitatable DNA is inhibited in cells exposed to YTR107 for 2 hours

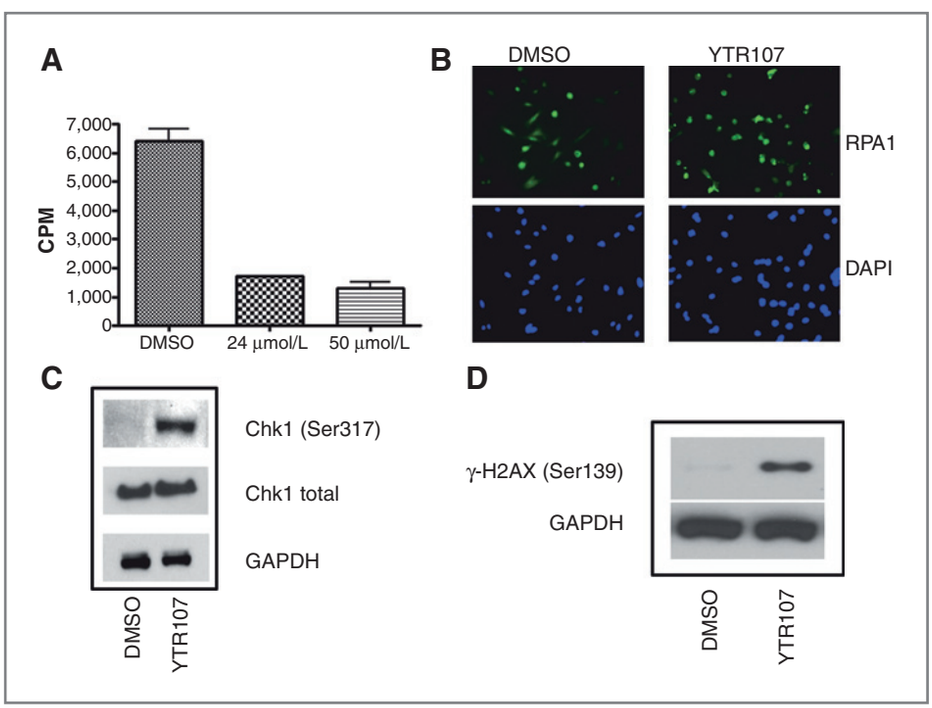

Figure 3. YTR107 induces replication stress in HT29 cells. A, cells were exposed to the indicated concentrations of YTR107 for 2 hours at 37°C. Cells were labeled with 8 μCi of [^{3}H]thymidine, washed, and DNA precipitated with ice-cold 10% trichloroacetic acid. Precipitated DNA was solubilized in 0.2N NaOH. [^{3}H]Thymidine incorporation was quantitated by scintillation counting; HT29 cells were exposed to 25 μmol/L YTR107 for 2 hours at 37°C and then analyzed for RPA2 immunofluoresence and DAPI counterstaining (B) or immunoblotted for pS317Chk1 and total Chk1 (C) or γH2AX and GAPDH (D). CPM, counts per minute.

Published OnlineFirst August 30, 2011; DOI:10.1158/1078-0432.CCR-11-1054

at 37°C ($P < 0.0001$, ANOVA). Inhibition of DNA synthesis can be accompanied by stalled DNA replication forks. Stalled replication forks result in accumulation of single-stranded regions. Replication protein A (RPA) binds to single-stranded DNA, and immunofluorescent imaging can be used to detect the presence of such regions (20). HeLa cells have excellent optical properties for immunofluorescent imaging and therefore were used to measure binding of RPA2 to single-stranded DNA following a 2-hour/25 μmol/L exposure to YTR107. Representative images are shown in Fig. 3B. Approximately 45% of control cells exhibited RPA immunofluorescent images that are characteristic of stage IB S-phase cells in which discrete replication foci have merged together (21). In contrast, approximately 65% of YTR-treated cells were immunofluorescence positive (Fig. 3B). Given that DNA synthesis is inhibited in YTR107-treated cells, we interpreted the increase in RPA immunofluorescence to be a consequence of increased regions of single-stranded DNA. RPA2 binding to single-stranded DNA results in recruitment of ATR (22) and subsequent ATR-mediated phosphorylation of Chk1 kinase at serine residues 317 and 345 (23). As shown in Fig. 3C, exposure to YTR107 produced a robust phosphorylation at Ser317 of Chk1.

Histone H2AX is phosphorylated at Ser139 in response to DNA DSBs. It is also phosphorylated in response to single-stranded DNA regions formed as a result of replication fork stalling (ref. 24 and references therein). Exposure to 25 μmol/L YTR107 for 2 hours resulted in H2AX phosphorylation in HT29 cells (Fig. 3D). Similar results were observed in MCF-7 cells (data not shown).

Chk1 signaling is essential for implementing the G2–M checkpoint (25). Consistent with the Chk1 and H2AX phosphorylation, cells accumulated in G2–M following exposure to YTR107 (2 hours/25 μmol/L; Supplementary Fig. S2). Taken together, the data presented in Fig. 3 and Supplementary Fig. S2 show that exposure to YTR107 is accompanied by inhibition of DNA synthesis, RPA binding to single-stranded DNA, ATR-mediated Chk1 phosphorylation, phosphorylation of H2AX, and activation of the G2–M check point. These events are the hallmark of an activated replication stress sensor–response pathway that is responding to stalled replication forks, as described by Branzei and Foiani (26).

We next determined whether YTR107 inhibited PARP activity. This was accomplished by measuring the ability of cell lysate obtained from cells exposed to 25 or 50 μmol/L YTR107 (2 hours/37°C) to catalyze the incorporation of biotinylated PARP into histone proteins in a 96-well format. We found that PARP activity derived from 50 μg cellular protein was independent of the YTR107 exposure (Supplementary Fig. S3).

Identification of NPM

To identify potential targets, both YTR107 and benzene (negative control) were linked to sepharose beads and allowed to bind total HT29 protein lysate. The structure of the linked YTR107 molecule is shown in Supplementary Fig. S4. Bound protein was stringently washed and eluted. Colloidal Coomassie Blue staining of SDS-PAGE–separated protein revealed the presence of YTR107-specific peptide bands that were excised, subjected to tryptic digestion, and analyzed by LS/MS-MS. The analysis revealed that the molecular chaperone NPM was one of the proteins captured by YTR107 immobilized to sepharose beads (53.4% sequence coverage; see Supplementary Fig. S5). The majority of the remaining proteins captured by the YTR107 resin were identified as proteins that can bind to NPM.

To confirm that YTR107 was binding to NPM, cellular protein lysate was added to biotinylated YTR107 or biotinylated benzoic acid (PNR-4-31) affinity beads (see Supplementary Fig. S4 for structures). Captured protein was washed, eluted, and subjected to immunoblotting with antibody to NPM. The immunoblot shown in Supplementary Fig. S6 illustrates that YTR107 affinity beads could trap NPM whereas biotinylated benzoic acid was not. The experiment was then repeated with purified recombinant NPM. Biotinylated YTR107, but not biotinylated benzoic acid, could capture recombinant NPM (Supplementary Fig. S6).

NSC348884 is a small molecule shown to disrupt NPM oligomerization and function (27). Exposure of HT29 cells to 10 μmol/L NSC348884 for 30 minutes before, during, and for 90 minutes after irradiation produced a statistically significant degree of radiosensitization (Supplementary Fig. S7A; $P < 0.04$, Student t test). In addition, siRNA targeting of NPM (SMARTpool from Dharmacon) was used to suppress NPM expression in HeLa cells. Control cells were transfected with a nontargeting siRNA. Cells were exposed to YTR107 and irradiated (Supplementary Fig. 7B). In cells transfected with control siRNA, YTR107 produced a statistically significant degree of radiosensitization ($P < 0.0001$). However, YTR107 failed to radiosensitize cells transfected with NPM siRNA ($P > 0.05$, Student t test).

Inhibition of NPM shuttling to sites of DNA DSBs in YTR107-treated cells

pT199-NPM has been shown to participate in repair of radiation-induced DSBs (16). Specifically, nucleoplasm-soluble pT199-NPM translocates into an insoluble chromatin fraction as it associates with BRCA1-BARD1 complexes at the sites of DNA DSBs. We monitored the solubility of pT199-NPM in irradiated cells by the biochemical fractionation technique described by Groisman and colleagues (19). Congruent with the results obtained by Koike and colleagues (16), pT199-NPM solubility decreased in irradiated cells. pT199-NPM solubility decreased by 50%, 90 minutes after administering 4 Gy, and by 60% following administration of 6 Gy (Fig. 4A). However, exposure to YTR107 before and after irradiation inhibited pT199-NPM redistribution.

Indirect immunofluorescent imaging by confocal microscopy was used to determine whether YTR107 affected NPM/γH2AX colocalization (Fig. 4B). HeLa cells were grown to 50% confluency, treated with YTR107 (50 μmol/L) for 30 minutes before exposure to 4 Gy, allowed to recover for 90 minutes at 37°C, and then analyzed by confocal

Published OnlineFirst August 30, 2011; DOI:10.1158/1078-0432.CCR-11-1054

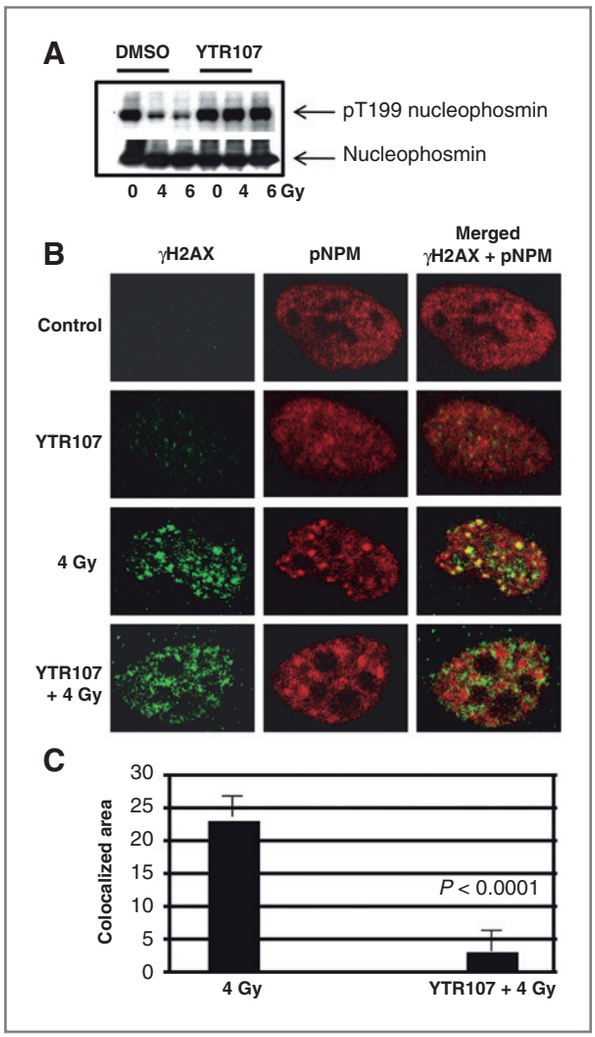

Figure 4. YTR107 inhibits pT199-NPM translocation to sites of DNA damage. A, nuclear extracts were prepared as described in Materials and Methods. Nonchromatin-bound protein immunoblotted for the presence of pT199-NMP. B, confocal images of cells stained for pT199-NPM and γH2AX. C, quantification of pNPM and γH2AX colocalization, as described in the text.

microscopy. While barely detectable in unirradiated cells, γH2AX (labeled with Alexa 488 (Green) was clearly detected 90 minutes after irradiation and exhibited a typical punctate pattern (Fig. 4B). Consistent with our previous observations, we saw some increase in γH2AX immunofluorescence in cells that were treated with YTR107 alone without irradiation (Fig. 4B). pT199-NPM [labeled with Alexa 647 (Red)] was detected in both normal and irradiated conditions (Fig. 4B).

Exposure to 4 Gy induced pT199-NPM colocalization with γH2AX (yellow color in the merged image, Fig. 4B). However, treatment with YTR107 markedly decreased this colocalization, as quantified using Metamorph software. The mean area of overlap between red pNPM signals and green γH2AX signals is a measure of colocalization and was calculated for cells exposed to 4 Gy with or without treatment with YTR107 (Fig. 4C). Data are expressed in arbitrary units (means ± SD) as the mean area overlap of red and green channels from 84 cells per condition. The data indicated a decrease in colocalization signal between pNPM and γH2AX in cells that were treated with YTR107 and irradiation ($P < 0.0001$, Student t test).

DNA DSB repair

The repair of DNA DSB induced by ionizing radiation is biphasic. Sixty percent of DSBs are repaired rapidly, with a rejoining half-life on the order of minutes (reviewed in ref. 28). The remaining DSBs are considered "persistent" and are repaired slowly, exhibiting rejoining half-lives on the order of hours.

Phosphorylation of histone H2AX at Ser139 represents one of the earliest events following the formation of DNA DSBs. Careful comparisons of γH2AX elimination kinetics with the kinetics of DNA DSB rejoining have shown a direct correlation between the number and repair of the "persistent" DNA DSBs and the formation and elimination of γH2AX (28).

We quantified γH2AX immunofluorescence 90 minutes after irradiation of HT29, PANC1, and H460 cells by flow cytometry. We found that γH2AX immunofluoresence was significantly elevated in irradiated HT29 and PANC1 cells exposed to YTR107 compared with cells irradiated in DMSO (solvent control; Supplementary Table S3). NSCLC H460 cells were irradiated in the presence of either DMSO or YTR107 and then incubated at 37°C for 1.5 or 2.5 hours before quantifying γH2AX immunofluoresence. Exposure to YTR107 slowed the elimination of γH2AX immunofluoresence, a surrogate for repair of DNA DSBs (Supplementary Table S4).

A neutral comet assay (29) was also used to assess the formation and repair of DNA DSBs following X-ray irradiation. HT29 cells were incubated at 37°C for 2 hours in the absence or presence of YTR107 (25 μmol/L), irradiated at 4°C, and then immediately processed for the comet assay (Fig. 5A–D). DNA DSBs were not detected in cells exposed to YTR107 alone (Fig. 5B). However, the comet heads from YTR107-treated cells did not yield sharp images (compare DMSO control, Fig. 5A, with 5B). This may be a consequence of YTR107-mediated replication stress that induced single-strand breaks. Exposure of cells to YTR107 before and during irradiation at 4°C, a temperature that inhibits repair, significantly increased comet tail length (compare Fig. 5C with 5D). These data indicate that the formation of radiation-induced DSBs was potentiated by YTR107.

HCC1806 breast adenocarcinoma cells are estrogen receptor negative, progesterone receptor negative, p53 null, and overexpress HER2/neu (30). The HCC1806 cells are radiosensitized by exposure to 25 μmol/L of YTR107 (Fig. 5E). The repair of DNA DSBs was quantified in these cells by measuring comet moment (Fig. 5F; defined in ref. 29). Cells were exposed to 25 μmol/L YTR107 for 30 minutes at 37°C, irradiated at 4°C, and immediately processed (at time 0: no repair) or allowed to repair at 37°C.

Published OnlineFirst August 30, 2011; DOI:10.1158/1078-0432.CCR-11-1054

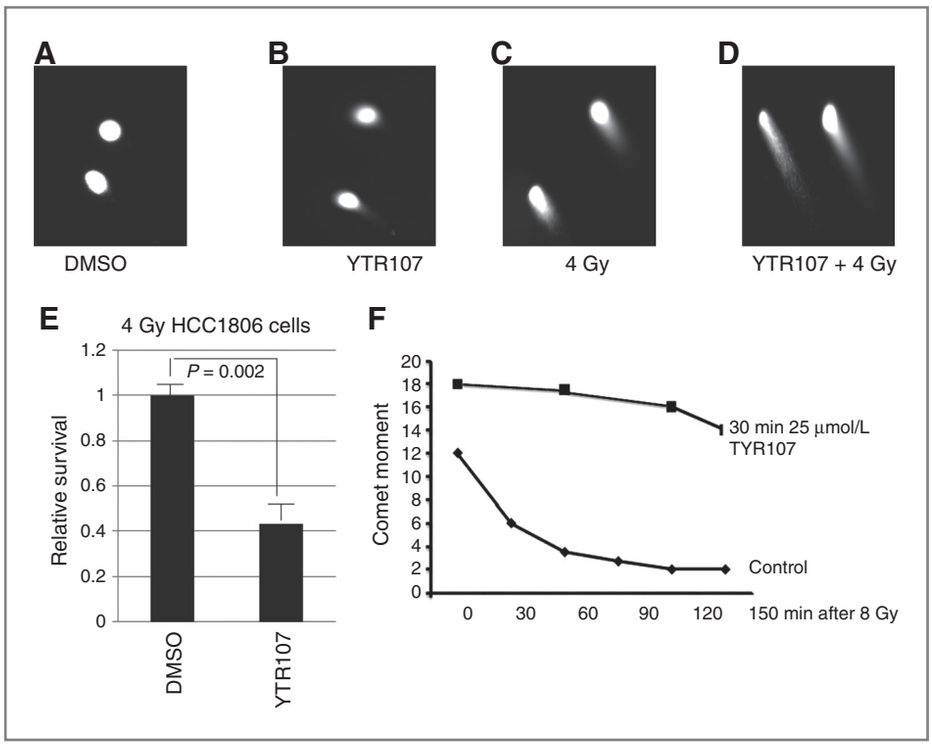

Figure 5. YTR107 inhibits repair of DNA DSBs. Cells were exposed to DMSO (A) or YTR107 (25 μmol/L; B) for 2 hours at 37°C and then administered 0 Gy (A and B) or 3 Gy (C and D) at 4°C. Immediately after irradiation, cells were subjected to a neutral comet assay. E, radiosensitization of HCC1809 cells by 25 μmol/L YTR107. Cells were exposed to YTR107 for 30 minutes before, during, and for 90 minutes after 4 Gy. F, the formation and repair of DNA DSBs of cells exposed to either DMSO or YTR107 for 30 minutes at 37°C, irradiated at 4°C, and allowed to repair at 37°C for up to 150 minutes.

These data show that in irradiated cells, YTR107 increased the formation of DNA DSBs and slowed their repair.

Discussion

The challenge to radiation oncology is to provide definitive local/regional control of tumors harboring complex genetic profiles. Comprehensive sequencing of cancer cell genomes has revealed a diversity of disease-specific mutations. Examples include *MLL2* mutations in medulloblastoma and *IDH1* mutations in glioblastoma (31, 32). In addition, the sequencing data have shown the presence of driver mutations that populate well-characterized signaling pathways that have established roles in oncogenesis and are common to many types of cancer (31). A collateral consequence of such oncogenic mutations is context-dependent resistance to therapeutic regimens.

We hypothesized that DNA damage response pathways harbor biological targets could be exploited for the purpose of producing context-independent sensitization. To test this hypothesis, we used a forward chemical genetics approach that used cell-based phenotypic screening of cancer cells for the purpose of identifying novel chemical entities (NCE) that could enhance therapeutic effectiveness. The screen identified YTR107, a 5-((*N*-benzyl-1*H*-indol-3-yl)methylene)pyrimidine-2,4,6(1*H*,3*H*,5*H*)trione as a compound that potentiated the radiation sensitivity of several diverse cancer cell lines and a HT29 xenograft.

YTR107 was used as a tool for identifying the biological target responsible for sensitization. One candidate protein identified was NPM, which is considered a chaperone that shuttles between various cellular compartments. Originally, it was described as a nucleolus protein involved in ribosome biogenesis (33). Recent research has shown that it is involved in many aspects of cell physiology (33). Emerging research has also shown that NPM participates in DNA damage responses. NPM is essential for embryonic development and maintenance of genomic stability (34, 35). Loss of NPM can induce replication stress. NPM copurifies with the DNA polymerase α–primase complex (36). Using purified and recombinant NPM in a cell-free system, Takemura and colleagues (36) have shown that NPM binds to and stimulates the activity of DNA polymerase α by as much as 3-fold. Thus, loss of NPM would be predicted to diminish DNA synthesis. Consistent with that hypothesis, Colombo and colleagues (34) found that RNA interference–mediated suppression of NPM in mouse embryo fibroblasts inhibited the incorporation of bromodeoxyuridine into DNA and induced cell-cycle arrest. Immunoblotting of $NPM^{-/-}$ embryo lysates indicated enhanced H2AX phosphorylation at Ser139 compared with lystates from wild-type embryos (34). The results reported in these studies provided a rationale for focusing on the role of NPM in YTR107-mediated radiosensitization.

Recently, Koike and colleagues, (16) found that pT199-NPM recruitment to sites of DNA DSBs is required for DNA repair. Recruitment relies upon the NPM ubiquitin binding motif-like domain interacting with an unknown substrate polyubiquitinated by RNF8 (16). RNF8 is recruited to sites of DNA damage via interaction with MDC1, allowing recruitment of BRCA1–Abraxas–RAP80 complexes. This event is followed by recruitment of BRCA2–RAD51

Published OnlineFirst August 30, 2011; DOI:10.1158/1078-0432.CCR-11-1054

complexes, thus licensing checkpoint signaling and homologous end joining (37). This DNA damage response pathway is initiated by both single-strand DNA regions produced by replication fork stalling and DNA DSBs. Failure to recruit NPM to this repair pathway stymies repair (16).

The use of an affinity-based solid-phase resin followed by LC-MS/MS or immunoblotting of captured protein showed the presence of NPM in the protein complex bound to YTR107. Confocal microscopy showed that pT199-NPM relocated to sites of DNA DSBs, denoted by γH2AX foci. We found that exposure to YTR107 prevented colocalization. Koike and colleagues (16) have shown that repair was inhibited when pT199-NPM failed to localize to sites of DNA DSBs. Similarly, radiation-induced DSB repair was inhibited in cells exposed to YTR107, coincident with failure of pT199-NPM to colocalize with γH2AX foci.

The increase in radiation sensitization, measured by a colony formation assay, which requires cells to undergo a minimum of 7 cell divisions, is consistent with an inhibition of DNA DSB repair. Although Koike and colleagues (16) did not observe a correlation between the 8-fold inhibition of DNA DSB repair and cell viability, this may be a consequence of the use of a colorimetric assay that measured viability 4 days after irradiation. Irradiated cancer cells can undergo up to 7 cell divisions prior to senescence, apoptosis, necrosis, or mitotic catastrophe (38, 39). Viability measurements made just 4 days after irradiation may not capture the full expression of cell death.

We also found that YTR107 produced a damage response similar to that produced by replication fork stalling: RPA coating of single-strand DNA, Chk1 phosphorylation by activated ATR, phosphorylation of the histone H2AX, followed by the activation of the G_2 checkpoint (20–23). The observation that YTR107 increased the initial level of DNA DSBs is interpreted to be a consequence of the interaction of the DNA single-strand breaks formed by replication stress with those generated by X-ray irradiation. Currently, it is not known whether YTR107-mediated "fork collapse" is a consequence of disregulated NPM. NPM regulates DNA polymerase α activity (36), which may be disrupted by YTR107. In addition, NPM is a well-characterized histone chaperone for the H2A–H2B histone dimer (reviewed in ref. 40) and histone organization requires chaperoning during DNA replication. Failure to correctly disassemble and reassemble histones during replication could be expected to induce a replication stress. Nucleosomes are also disrupted during the repair of DNA DSBs (discussed in ref. 41). Thus, one may hypothesize that YTR107-mediated disruption of NPM-mediated histone chaperone activity results in replication fork stalling and inhibition of DNA strand break repair. Alternatively, YTR107-mediated replication fork stress may be independent of NPM because Koike and colleagues (16) did not report replication fork collapse in cells expressing T199A-NPM. Future research will determine the answer to this question.

In summary, these data support the hypothesis that YTR107 inhibits the repair of DNA DSBs by deregulation of NPM shuttling and identify this pathway as a potential target for enhancing the efficacy of DNA-damaging therapeutic strategies in cells harboring *RAS*, *BRAF*, *ErbB*, and/or *PIK3CA* driver mutations/amplifications.

Disclosure of Potential Conflicts of Interest

K.R. Sekhar, Y.T. Reddy, P.N. Reddy, P.A. Crooks, and M.L. Freeman have filed a patent application for YTR107.

Grant Support

The study was supported in part by grants from U.S. NI Health/National Cancer Institute grants RO1CA140409, T32CA093240, and P50CA095103 and Vanderbilt-Ingram Cancer Center grant P30 CA68485.

The costs of publication of this article were defrayed in part by the payment of page charges. This article must therefore be hereby marked *advertisement* in accordance with 18 U.S.C. Section 1734 solely to indicate this fact.

Received April 20, 2011; revised July 13, 2011; accepted July 30, 2011; published OnlineFirst August 30, 2011.

References

1. Luo J, Solimini NL, Elledge SJ. Principles of cancer therapy: oncogene and non-oncogene addiction. Cell 2009;136:823–37.
2. National Comprehensive Cancer Network Inc. [cited 2011]. Available from: http://wwwnccnorg/professionals/physician_gls/f_guidelinesasp#site.
3. Jeggo P, Lavin MF. Cellular radiosensitivity: how much better do we understand it? Int J Radiat Biol 2009;85:1061–81.
4. Davies KJ. Protein damage and degradation by oxygen radicals. I. general aspects. J Biol Chem 1987;262:9895–901.
5. Sartor CI. Epidermal growth factor family receptors and inhibitors: radiation response modulators. Semin Radiat Oncol 2003;13:22–30.
6. Chen H, Ma Z, Vanderwaal RP, Feng Z, Gonzalez-Suarez I, Wang S, et al. The mTOR inhibitor rapamycin suppresses DNA double-strand break repair. Radiat Res 2011;175:214–24.
7. Bozic I, Antal T, Ohtsuki H, Carter H, Kim D, Chen S, et al. Accumulation of driver and passenger mutations during tumor progression. Proc Natl Acad Sci U S A 2010;107:18545–50.
8. Dahabreh IJ, Terasawa T, Castaldi PJ, Trikalinos TA. Systematic review: Anti-epidermal growth factor receptor treatment effect modification by KRAS mutations in advanced colorectal cancer. Ann Intern Med 2011;154:37–49.
9. McKenna WG, Weiss MC, Endlich B, Ling CC, Bakanauskas VJ, Kelsten ML, et al. Synergistic effect of the v-myc oncogene with H-ras on radioresistance. Cancer Res 1990;50:97–102.
10. Yao TW, Kim WS, Yu DM, Sharbeen G, McCaughan GW, Choi KY, et al. Targeting epidermal growth factor receptor-associated signaling pathways in non-small cell lung cancer cells: implication in radiation response. Mol Cancer Res 2011;8:1027–36.
11. Bao S, Wu Q, McLendon RE, Hao Y, Shi Q, Hjelmeland AB, et al. Glioma stem cells promote radioresistance by preferential activation of the DNA damage response. Nature 2006;444:756–60.
12. Gangadhar NM, Stockwell BR. Chemical genetic approaches to probing cell death. Curr Opin Chem Biol 2007;11:83–7.
13. Reddy YT, Sekhar KR, Sasi N, Reddy PN, Freeman ML, Crooks PA. Novel substituted (*Z*)-5-((*N*-benzyl-1*H*-indol-3-yl)methylene)imidazolidine-2,4-diones and 5-((*N*-benzyl-1*H*-indol-3-yl)methylene)pyrimidine-2,4,6(1*H*,3*H*,5*H*)-triones as potent radio-sensitizing agents. Bioorg Med Chem Lett 2010;20:600–2.
14. Palmer RH, Vernersson E, Grabbe C, Hallberg B. Anaplastic lymphoma kinase: signalling in development and disease. Biochem J 2009;420:345–61.

Published OnlineFirst August 30, 2011; DOI:10.1158/1078-0432.CCR-11-1054

15. Brady SN, Maggi LB, Winkeler CL, Toso EA, Gwinn AS, Pelletier CL, et al. Nucleophosmin protein expression level, but not threonine 198 phosphorylation, is essential in growth and proliferation. Oncogene 2009;28:3209–20.
16. Koike A, Nishikawa H, Wu W, Okada Y, Venkitaraman AR, Ohta T. Recruitment of phosphorylated NPM1 to sites of DNA damage through RNF8-dependent ubiquitin conjugates. Cancer Res 2010;70:6746–56.
17. Geng L, Rachakonda G, Morré DJ, Morré DM, Crooks PA, Sonar VN, et al. Indolyl-quinuclidinols inhibit ENOX activity and endothelial cell morphogenesis while enhancing radiation-mediated control of tumor vasculature. FASEB J 2009;23:2986–95.
18. Franken NA, Rodermond HM, Stap J, Haveman J, van Bree C. Clonogenic assay of cells *in vitro*. Nat Protoc 2006;1:2315–9.
19. Groisman R, Polanowska J, Kuraoka I, Sawada J, Saijo M, Drapkin R, et al. The ubiquitin ligase activity in the DDB2 and CSA complexes is differentially regulated by the COP9 signalosome in response to DNA damage. Cell 2003;113:357–67.
20. Dart DA, Adams KE, Akerman I, Lakin ND. Recruitment of the cell cycle checkpoint kinase ATR to chromatin during S-phase. J Biol Chem 2004;279:16433–40.
21. Dimitrova DS, Berezney R. The spatio-temporal organization of DNA replication sites is identical in primary, immortalized and transformed mammalian cells. J Cell Sci 2002;115:4037–51.
22. Choi JH, Lindsey-Boltz LA, Kemp M, Mason AC, Wold MS, Sancar A. Reconstitution of RPA-covered single-stranded DNA-activated ATR-Chk1 signaling. Proc Natl Acad Sci U S A 2010;107:13660–5.
23. Zhao H, Piwnica-Worms H. ATR-mediated checkpoint pathways regulate phosphorylation and activation of human Chk1. Mol Cell Biol 2001;21:4129–39.
24. Fragkos M, Jurvansuu J, Beard P. H2AX is required for cell cycle arrest via the p53/p21 pathway. Mol Cell Biol 2009;29:2828–40.
25. Liu Q, Guntuku S, Cui XS, Matsuoka S, Cortez D, Tamai K, et al. Chk1 is an essential kinase that is regulated by Atr and required for the G(2)/M DNA damage checkpoint. Genes Dev 2000;14:1448–59.
26. Branzei D, Foiani M. The checkpoint response to replication stress. DNA Repair (Amst) 2009;8:1038–46.
27. Qi W, Shakalya K, Stejskal A, Goldman A, Beeck S, Cooke L, et al. NSC348884, a nucleophosmin inhibitor disrupts oligomer formation and induces apoptosis in human cancer cells. Oncogene 2008;27:4210–20.
28. Svetlova MP, Solovjeva LV, Tomilin NV. Mechanism of elimination of phosphorylated histone H2AX from chromatin after repair of DNA double-strand breaks. Mutat Res 2010;685:54–60.
29. Olive PL, Banath JP, Durand RE. Heterogeneity in radiation-induced DNA damage and repair in tumor and normal cells measured using the "comet" assay. Radiat Res 1990;122:86–94.
30. Gazdar AF, Kurvari V, Virmani A, Gollahon L, Sakaguchi M, Westerfield M, et al. Characterization of paired tumor and non-tumor cell lines established from patients with breast cancer. Int J Cancer 1998;78:766–74.
31. Parsons DW, Jones S, Zhang X, Lin JC, Leary RJ, Angenendt P, et al. An integrated genomic analysis of human glioblastoma multiforme. Science 2008;321:1807–12.
32. Parsons DW, Li M, Zhang X, Jones S, Leary RJ, Lin JC, et al. The genetic landscape of the childhood cancer medulloblastoma. Science 2011;331:435–9.
33. Grisendi S, Mecucci C, Falini B, Pandolfi PP. Nucleophosmin and cancer. Nat Rev Cancer 2006;6:493–505.
34. Colombo E, Bonetti P, Lazzerini Denchi E, Martinelli P, Zamponi R, Marine JC, et al. Nucleophosmin is required for DNA integrity and p19Arf protein stability. Mol Cell Biol 2005;25:8874–86.
35. Grisendi S, Bernardi R, Rossi M, Cheng K, Khandker L, Manova K, et al. Role of nucleophosmin in embryonic development and tumorigenesis. Nature 2005;437:147–53.
36. Takemura M, Ohta N, Furuichi Y, Takahashi T, Yoshida S, Olson MO, et al. Stimulation of calf thymus DNA polymerase alpha activity by nucleolar protein B23. Biochem Biophys Res Commun 1994;199:46–51.
37. Bekker-Jensen S, Mailand N. Assembly and function of DNA double-strand break repair foci in mammalian cells. DNA Repair (Amst) 2010;9:1219–28.
38. Bedford JS, Mitchell JB, Griggs HG, Bender MA. Radiation-induced cellular reproductive death and chromosome aberrations. Radiat Res 1978;76:573–86.
39. Chu K, Leonhardt EA, Trinh M, Prieur-Carrillo G, Lindqvist J, Albright N, et al. Computerized video time-lapse (CVTL) analysis of cell death kinetics in human bladder carcinoma cells (EJ30) X-irradiated in different phases of the cell cycle. Radiat Res 2002;158:667–77.
40. Eitoku M, Sato L, Senda T, Horikoshi M. Histone chaperones: 30 years from isolation to elucidation of the mechanisms of nucleosome assembly and disassembly. Cell Mol Life Sci 2008;65:414–44.
41. Kastan MB. DNA damage responses: mechanisms and roles in human disease: 2007 G.H.A. Clowes Memorial Award Lecture. Mol Cancer Res 2008;6:517–24.